AGU PUBLICATIONS

Geophysical Research Letters

RESEARCH LETTER
10.1002/2015GL065805

Key Points:
- MESSENGER observations revealed solar wind plasma transported deep into Mercury's magnetotail
- Mercury's plasma mantle is identified as a main region for solar wind entry into the magnetosphere
- Flux transfer events deliver solar wind plasma into the high-latitude magnetotail

Correspondence to:
G. A. DiBraccio,
gdibracc@umich.edu

Citation:
DiBraccio, G. A., et al. (2015), First observations of Mercury's plasma mantle by MESSENGER, *Geophys. Res. Lett.*, *42*, 9666–9675, doi:10.1002/2015GL065805.

Received 14 AUG 2015
Accepted 23 SEP 2015
Accepted article online 28 SEP 2015
Published online 25 NOV 2015

©2015. American Geophysical Union. All Rights Reserved.

First observations of Mercury's plasma mantle by MESSENGER

Gina A. DiBraccio[1,2], James A. Slavin[1], Jim M. Raines[1], Daniel J. Gershman[3,4], Patrick J. Tracy[1], Scott A. Boardsen[4,5], Thomas H. Zurbuchen[1], Brian J. Anderson[6], Haje Korth[6], Ralph L. McNutt Jr.[6], and Sean C. Solomon[7,8]

[1]Department of Atmospheric, Oceanic and Space Sciences, University of Michigan, Ann Arbor, Michigan, USA, [2]Solar System Exploration Division, NASA Goddard Space Flight Center, Greenbelt, Maryland, USA, [3]Geospace Physics Laboratory, NASA Goddard Space Flight Center, Greenbelt, Maryland, USA, [4]Goddard Planetary Heliophysics Institute, University of Maryland, Baltimore County, Baltimore, Maryland, USA, [5]Heliophysics Science Division, NASA Goddard Space Flight Center, Greenbelt, Maryland, USA, [6]The Johns Hopkins University Applied Physics Laboratory, Laurel, Maryland, USA, [7]Lamont-Doherty Earth Observatory, Columbia University, Palisades, New York, USA, [8]Department of Terrestrial Magnetism, Carnegie Institution of Washington, Washington, District of Columbia, USA

Abstract We present the first observations of Mercury's plasma mantle, a primary region for solar wind entry into the planetary magnetosphere, located in the high-latitude magnetotail. MErcury Surface, Space ENvironment, GEochemistry, and Ranging (MESSENGER) observations from two orbits on 10 November 2012 have been analyzed. The main plasma mantle features are (1) a steady decrease in proton density as MESSENGER moved deeper into the magnetotail; (2) frequent flux transfer events throughout the magnetosheath and into the magnetotail, suggesting that these events are the primary source for solar wind plasma injection; (3) a diamagnetic depression, due to the presence of plasma, as pressure balance is maintained; and (4) a clear proton velocity dispersion, resulting from lower-energy protons being transported deep into the magnetosphere as higher-energy protons escape downtail. From these velocity dispersions we infer cross-magnetosphere electric potentials of 23 kV and 29 kV, consistent with estimates determined from measurements of magnetopause reconnection rate and tail loading and unloading events.

1. Introduction

Mercury's magnetosphere is formed by the interaction of the Sun's supersonic, super-Alfvénic solar wind with the planet's intrinsic magnetic field. Prior to the MErcury Surface, Space ENvironment, GEochemistry, and Ranging (MESSENGER) mission, our understanding of this dynamic magnetosphere was restricted to in situ measurements from two of the three flybys of the Mariner 10 spacecraft and limited ground-based observations [*Ness et al.*, 1974, 1975; *Ogilvie et al.*, 1974, 1977; *Simpson et al.*, 1974; *Potter and Morgan*, 1985, 1986]. Initially, it appeared that Mercury's magnetosphere was a miniature version of Earth's, operating in much the same manner. However, MESSENGER observations indicate that this planetary environment is anything but ordinary.

The combination of Mercury's proximity to the Sun, frequent occurrence of intense magnetopause reconnection [*DiBraccio et al.*, 2013], and lack of a conducting ionosphere leads to a rapid circulation of plasma and magnetic flux, as predicted by *Hill et al.* [1976]. Large-scale magnetospheric convection, termed the Dungey cycle, has a characteristic timescale of only ~2 min at Mercury [*Slavin et al.*, 2009, 2010] compared with ~1 h at Earth [*Siscoe et al.*, 1975]. Mercury's short Dungey cycle implies that plasma, of both solar and planetary origins, is continuously undergoing rapid circulation.

Throughout the Dungey cycle, the interplanetary magnetic field (IMF) merges with planetary field lines, via magnetic reconnection at the dayside magnetopause, to create newly open field lines that convect around the planet, joining the magnetotail and facilitating the entry of solar wind plasma. Any plasma populating the magnetic field, **B**, in the high-latitude tail will $\mathbf{E} \times \mathbf{B}$ drift toward the equatorial plasma sheet as a result of the cross-magnetosphere electric field, **E**. Therefore, the Dungey cycle provides two linked channels through which the solar wind may enter the magnetosphere: (1) along newly open flux tubes, following dayside reconnection, providing direct access into the magnetic cusps, where the ions and electrons may mirror or impact the surface, and (2) through open field lines that are transferred to the magnetotail, carrying any plasma populating the fields across the magnetopause.

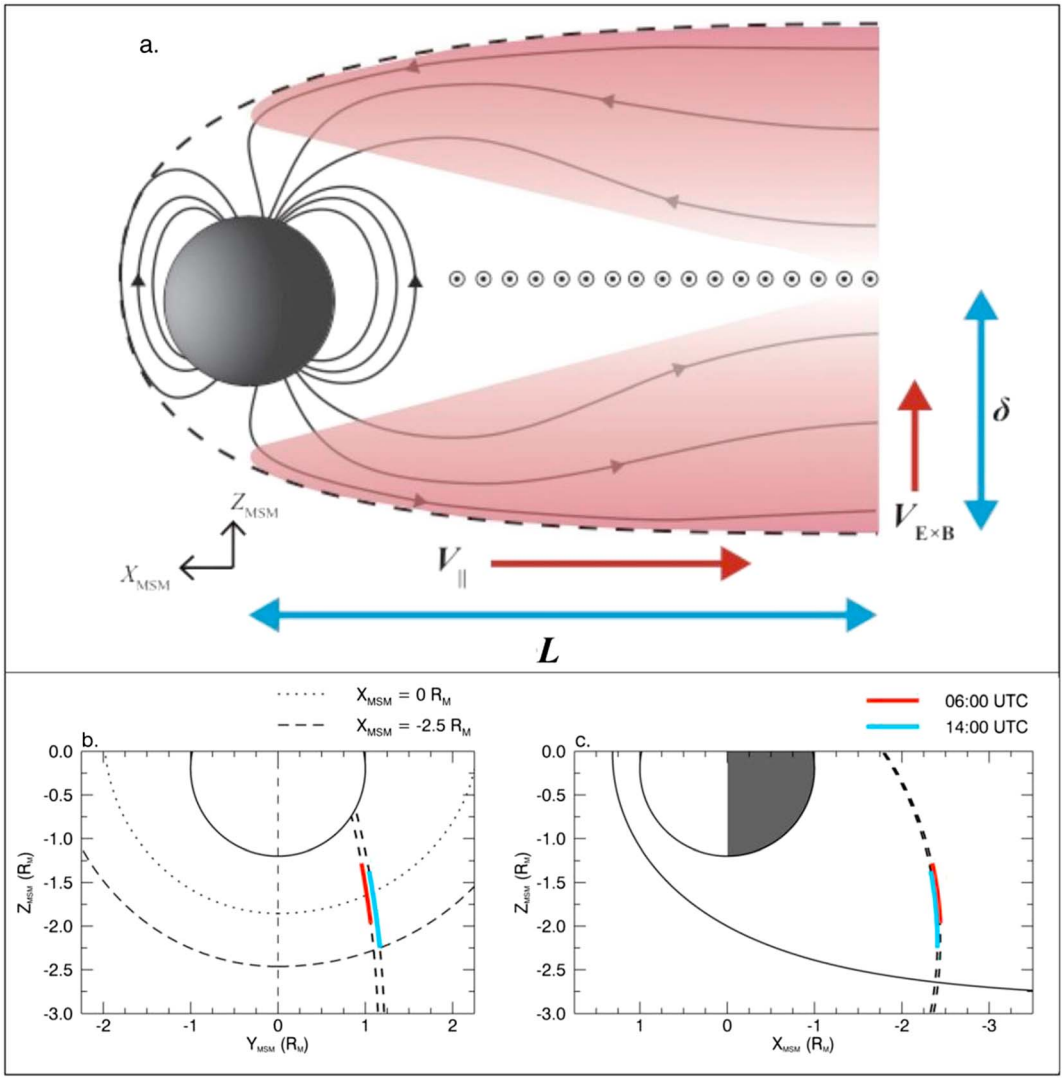

Figure 1. (a) Schematic illustration of Mercury's magnetosphere and plasma mantle (shaded red). Magnetospheric regions include the planetary magnetic field (black lines with arrows), the model magnetopause boundary (dashed line), and the cross-tail current sheet (circle with dot). Directions of solar wind velocity parallel to the magnetic field ($\mathbf{V}_{||}$) and resulting from the $\mathbf{E}\times\mathbf{B}$ drift ($\mathbf{V}_{E\times B}$) are shown. Plasma mantle length and thickness are denoted by L and δ, respectively. (b) View from the Sun for which the model magnetopause location is indicated at $X_{MSM} = 0\ R_M$ (dotted line) and $X_{MSM} = -2.5\ R_M$ (thin dashed line). (c) Meridional view for which the model magnetopause location is indicated by the solid line. In Figures 1b and 1c, MESSENGER orbits on 10 November 2012 are shown in MSM coordinates as thick dashed lines. Portions of the orbit trajectory when the plasma mantle was observed are highlighted for the 07:45 (red) and 15:45 UTC (blue) orbits.

In the latter case, a boundary layer forms as open field lines carry the solar wind plasma into the magnetotail. This boundary layer, known as the plasma mantle, is a thick region of magnetosheath-like plasma flowing antisunward inside the high-latitude magnetotail, adjacent to the magnetopause (Figure 1a) [*Rosenbauer et al.*, 1975; *Pilipp and Morfill*, 1978]. The charged particles of the plasma mantle follow trajectories that are the sum of this antisunward, magnetic field-aligned flow, $\mathbf{V}_{||}$, and the $\mathbf{E}\times\mathbf{B}$ drift, $\mathbf{V}_{E\times B}$, perpendicular to the magnetic field, creating a net motion toward the central plasma sheet. The particles with lower $V_{||}$ reach the plasma sheet closer to the planet, whereas those with higher $V_{||}$ arrive at much greater downtail distances. For example, at Earth, plasma mantle particles with the lowest $V_{||}$ join the plasma sheet at distances of 30–40 R_E (where R_E is Earth's radius) downstream of the planet, whereas those with higher field-aligned speeds arrive at distances $\geq$100 R_E [*Rosenbauer et al.*, 1975; *Pilipp and Morfill*, 1978; *Sckopke and Paschmann*, 1978; *Slavin et al.*, 1985]. This difference in particle velocity causes the plasma mantle thickness to expand

with increasing downtail distance (Figure 1a). For this reason, magnetohydrodynamic models characterize the plasma mantle as a "slow-mode expansion fan" [e.g., *Siscoe and Sanchez*, 1987].

At Earth, the presence of a dense plasma mantle has been correlated with southward IMF, and it is observed to vanish during extended periods of northward IMF, confirming that it is reconnection-driven [*Sckopke et al*., 1976; *Sckopke and Paschmann*, 1978]. *Sibeck and Siscoe* [1984] argued that flux transfer events (FTEs), discrete helical bundles of magnetic flux produced by simultaneous multiple X-line reconnection occurring along the dayside magnetopause, are an important source of the plasma mantle. As a vehicle for plasma exchange, FTEs facilitate the mixing of magnetosheath and magnetospheric particles [*Russell and Elphic*, 1978, 1979; *Daly et al*., 1981]. For this reason, they are observed to have densities and temperatures intermediate to those of the adjacent magnetosphere and magnetosheath regions [e.g., *Paschmann et al*., 1982; *Le et al*., 2008].

Unlike at Earth, FTEs play a major role in driving magnetospheric dynamics at Mercury [*Slavin et al*., 2008, 2009, 2010; *Imber et al*., 2014]. *Slavin et al*. [2012] reported observations of an "FTE shower" along the tail magnetopause, including a ~25 min interval of continuous flux rope encounters, with durations lasting only ~2–3 s and separations of ~8–10 s between individual events. This observation of frequent FTE transport into Mercury's tail suggests that these structures may directly supply Mercury's plasma mantle.

We present the first observations of Mercury's plasma mantle. Until now, this boundary layer has been directly observed only in Earth's magnetosphere [*Rosenbauer et al*., 1975]. From MESSENGER plasma and magnetic field measurements, we have selected two successive orbits on 10 November 2012 for detailed analysis on the basis of a high flux of solar wind protons just inside the high-latitude magnetotail. For both of these events, the velocity dispersion in the proton energy distributions, the defining feature of the plasma mantle at Earth [e.g., *Pilipp and Morfill*, 1978], is observed and analyzed. Frequent FTEs, observed throughout the magnetosheath-magnetopause interface for both cases, indicate that newly opened magnetic flux is continuously augmenting the high-latitude tail and delivering magnetosheath plasma to the plasma mantle.

2. Instrumentation and Data

In this study we analyzed MESSENGER Fast Imaging Plasma Spectrometer (FIPS) [*Andrews et al*., 2007] proton measurements at the full 10 s resolution and Magnetometer (MAG) [*Anderson et al*., 2007] data at its maximum sampling rate of 20 vectors per second.

FIPS measured ions with energy-per-charge (E/q) ratios of 0.046–13.3 keV/e and mass-per-charge ratios up to 60 amu/e. The instantaneous field of view (FOV) of FIPS was 1.4π sr, but approximately 0.25π sr was blocked by MESSENGER's sunshade. The sensor had an approximate angular resolution of 15°. Plasma moments are not used in this analysis because of the difficulty of deriving them from the sensor's limited FOV in this flow velocity regime. *Raines et al*. [2011, 2013] and *Gershman et al*. [2012, 2013] have provided further details regarding FIPS plasma measurements and instrument constraints.

To evaluate plasma characteristics in Mercury's plasma mantle, we utilized the three-dimensional proton angular and energy distributions derived from FIPS observations. Additionally, we created histograms of proton flow direction, called angular flux maps, by transforming FIPS observations into a discrete non-detector-based coordinate system. We used 10° angular bins to match the digital resolution of FIPS angular measurements. After rebinning the histograms in the new coordinate system, each bin need not have been sampled for the same duration. To adjust for this heterogeneity, a bin-dependent time normalization, derived from the total accumulation time of each visible pixel on the FIPS detector, was applied to the histograms. *Raines et al*. [2014] and *Gershman et al*. [2014] provided additional information on the derivation of angular flux maps and energy distributions.

3. Plasma Mantle Observations

Plasma mantle events were observed during two orbits on 10 November 2012, designated by periapsis times of approximately 07:45 UTC and 15:45 UTC. For these particular orbits, MESSENGER's orbital period was 8 h and periapsis was on Mercury's dayside, near 07:30 local time (Figures 1b and 1c). Portions of the orbit trajectories, along with the average magnetopause location [*Winslow et al*., 2013], are displayed in Mercury solar magnetospheric (MSM) coordinates in Figures 1b and 1c. In the MSM coordinate system, the X_{MSM} axis

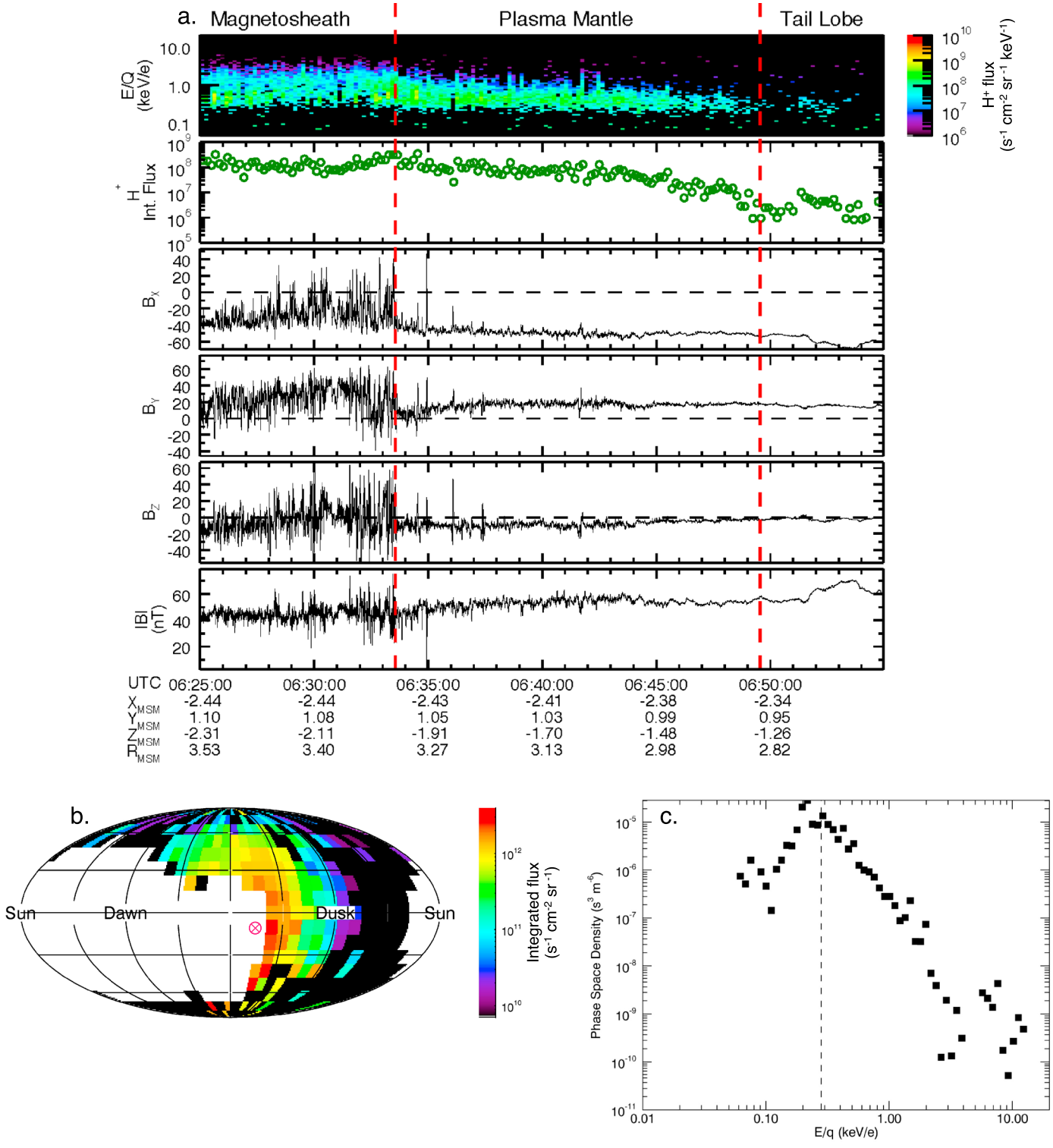

Figure 2. MESSENGER measurements taken during the inbound magnetopause crossing during the 07:45 UTC orbit on 10 November 2012. (a) FIPS and MAG time series data: (from top to bottom) proton energy spectrogram (units of flux: s^{-1} cm^{-2} sr^{-1} keV^{-1}); proton flux (s^{-1} cm^{-2}); magnetic field components B_X, B_Y, and B_Z; and total field magnitude B. The vertical dashed red lines mark the beginning and end of the plasma mantle at the magnetopause crossing and the termination of the plasma dispersion, respectively, with magnetospheric regions labeled at the top. (b) Angular flux map (units of integrated flux: s^{-1} cm^{-2} sr^{-1}) indicating proton flow directions. Average magnetic field direction is indicated by the pink circle-with-cross symbol. White bins are outside the FIPS FOV, and black bins have no measurements. (c) Phase space density as a function of E/q. The vertical dashed line marks the weighted average energy of observed protons, calculated by placing greater importance on measurements with higher flux.

is directed from Mercury's offset magnetic dipole toward the center of the Sun, the Z_{MSM} axis is normal to Mercury's orbital plane and positive northward, and the Y_{MSM} axis completes the right-handed system.

During these noon-midnight orbits, the spacecraft was located in the pre-midnight sector as it entered the magnetosphere at distances of several R_M (where R_M is Mercury's radius, or 2440 km) behind the planet before continuing through the southern tail lobe, approaching the central plasma sheet. The spacecraft orientation enabled FIPS to observe plasma flowing antisunward and duskward, which is ideal for plasma mantle flows in this region. We note that spacecraft rotations occurred during the intervals reported here, but they do not affect our assessment of the plasma mantle. The two plasma mantle examples presented here were chosen on the basis of their pristine signatures, resulting from the optimal viewing orientation of the FIPS sensor combined with the spacecraft's orbital trajectory that provided measurements at downtail distances $>2\,R_M$.

3.1. 10 November 2012: 07:45 UTC Orbit

During the first orbit on 10 November 2012, MESSENGER crossed the tail bow shock at ~05:09 UTC at a radial distance of 4.89 R_M from the planet. The magnetopause was encountered ~90 min later at 06:33:35 UTC when the spacecraft was located at a radial distance of 3.30 R_M. Figure 2a provides a 30 min overview of observations from the tail magnetosheath into Mercury's southern tail lobe, defined as the region of open field lines that form the magnetotail.

In the magnetosheath, the IMF was predominantly in the $-B_X$ and $+B_Y$ directions, with $B \sim 46$ nT. The high-frequency magnetic field variations are FTEs that were formed at the dayside magnetopause by reconnection [*Slavin et al.*, 2012; *Imber et al.*, 2014] and pulled into the tail as part of the Dungey cycle convection. We have confirmed these structures to be FTEs on the basis of their bipolar signatures, signifying a helical field topology, coincident with a field magnitude enhancement indicative of a strong axial core field, in the MAG data. FIPS magnetosheath measurements indicate a constant spread in proton energies and a peak energy of 0.39 keV, corresponding to a solar wind speed of ~275 km s^{-1}. The proton flux remained relatively constant at ~10^8 s^{-1} cm^{-2}.

The tail magnetopause crossing (first vertical dashed red line, Figure 2a) is identified by a rotation in all three MAG components along with an overall reduction in FTE activity, a shift in the plasma energy distribution, and a decrease in proton flux. Despite these shifts in the FIPS data, the observed plasma remained continuous and had characteristics similar to those of the magnetosheath population; therefore, we infer that we observed magnetosheath plasma that had entered the magnetosphere. The total field magnitude remained relatively constant across the boundary, indicating that plasma and magnetic field pressures did not change significantly and that the boundary was likely a rotational discontinuity.

The 16 min interval between the vertical dashed red lines in Figure 2a, from 06:33:35 to 06:49:33 UTC, marks the region just inside Mercury's tail magnetopause where solar wind plasma was observed to form Mercury's plasma mantle. High proton fluxes, with characteristics intermediate to those of the adjacent magnetosheath and magnetosphere, were seen throughout the plasma mantle. The mantle's main feature is the proton energy dispersion, confirming the transition from solar wind magnetosheath-like plasma to planetary magnetosphere-like plasma. This transition was observed as the proton flux steadily decreased from ~10^8 s^{-1} cm^{-2}, analogous to magnetosheath observations, to ~10^6 s^{-1} cm^{-2} in the magnetotail lobe. This dispersive transition of solar wind plasma with distance from the magnetopause is due to the inward $\mathbf{E}\times\mathbf{B}$ drift of low-$V_{||}$ protons toward the central plasma sheet while those with higher $V_{||}$ escape farther downtail. Because of MESSENGER's trajectory, the low-energy particles were continuously measured while the observed upper limit of particle energy decreased with decreasing latitude. This plasma wedge feature is evident between the vertical dashed lines in the energy spectrogram of Figure 2a.

Throughout the plasma mantle, B increased from 46 nT to 60 nT as the plasma dispersed. The field orientation was primarily in the $-B_X$ direction, indicative of the antisunward-directed field in the southern lobe. FTE signatures are identified along the extent of the plasma mantle as a mechanism for delivering solar wind particles into the magnetosphere. Passing FTEs may also be detected indirectly in the lobe by the presence of locally compressed fields that drape around an FTE moving downtail, known as a traveling compression region (TCR) [*Slavin et al.*, 2012].

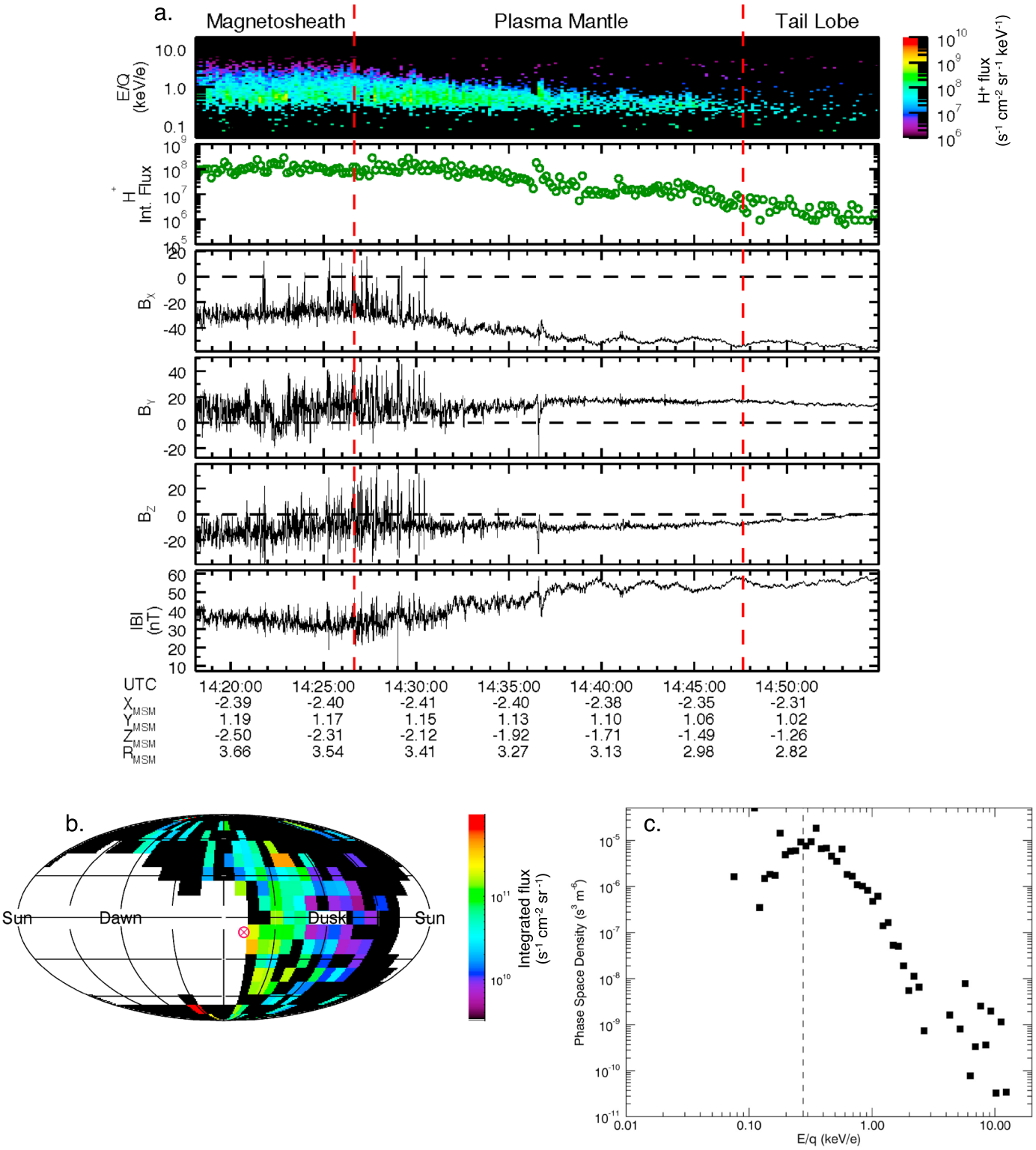

Figure 3. MESSENGER FIPS and MAG measurements taken during the 15:45 UTC orbit on 10 November 2012. The plots and format follow those of Figure 2.

The accumulation of three-dimensional FIPS proton measurements in the plasma mantle is displayed in Figures 2b and 2c. The angular flux map (Figure 2b) represents the flow direction, in MSM coordinates, at the location of the spacecraft, with the center corresponding to the antisunward direction. During this plasma mantle encounter, the magnetic field vector was near the edge of the FIPS FOV; however, the proton distribution peaked around the magnetic field direction, suggesting a field-aligned flow in the antisunward direction. This type of flow pattern is expected for solar wind plasma entering the magnetotail along open field lines and is consistent with Earth observations. Figure 2c shows proton energy distribution slices summed over the duration of the plasma mantle with a peak at 0.28 keV, indicating a speed of ~230 km s^{-1}.

The plasma mantle had diminished by 06:49:33 UTC, observed as the discrete reduction in proton energy as the decrease in proton flux simultaneously subsided. MESSENGER was well within the southern lobe and located at a radial distance of 2.83 R_M. Only very low proton fluxes were detected, which is typical of the low values of β, the ratio of thermal to magnetic pressure, in the tail lobes, and the magnetic field was quiet without the presence of FTEs. The dominant $-B_X$ component measured ~50 nT, with a slight influence of ~15 nT in the B_Y direction.

3.2. 10 November 2012: 15:45 UTC Orbit

During the second orbit on 10 November 2012, MESSENGER encountered the tail bow shock at ~13:36 UTC, when the spacecraft was positioned 4.52 R_M from the planetary center. As on the previous orbit, the magnetosheath was heavily populated by FTEs moving downtail. A 35 min overview of MAG and FIPS measurements is displayed in Figure 3a. The magnetosheath solar wind proton energy has a weighted average of ~0.45 keV, corresponding to a velocity of ~295 km s^{-1}. The magnetosheath proton flux was ~10^8 s^{-1} cm^{-2}, and the IMF was orientated primarily in the $-B_X$ direction, with B ~ 34 nT.

A dense proton population forming the plasma mantle was present for a 21 min interval after the magnetopause crossing. With signatures similar to those of the previous orbit, the energy distribution of the solar wind inside the high-latitude magnetotail began to disperse with increasing distance from the magnetopause. At the outer edge of the plasma mantle, proton energies were identical to those of the magnetosheath solar wind. However, as measurements progressed away from the magnetopause, a clear dispersion in the proton energy was observed as the high-$V_{||}$ protons escaped farther down the tail along the open field lines.

The proton fluxes decreased as MESSENGER moved through the mantle from initial measurements of ~10^8 s^{-1} cm^{-2}, equivalent to magnetosheath values, to ~10^6 s^{-1} cm^{-2}, comparable to values in the tail lobe. This decreasing plasma pressure means that the plasma's diamagnetic effect also diminished, causing B to increase simultaneously. Just inside the magnetopause, B was ~34 nT. The field magnitude increased to ~57 nT and became relatively constant thereafter. Large-amplitude FTEs were prevalent throughout the extent of the plasma mantle until ~14:30:30 UTC. At that time, the spacecraft recorded bipolar signatures of lower magnitude, which were the TCR signatures of locally compressed lobe fields as FTEs passed by. Once again, this pattern suggests that FTEs are responsible for supplying the mantle with solar wind plasma.

The average proton kinetic properties measured by FIPS are presented in Figures 3b and 3c. The angular flux map in Figure 3b indicates that the average magnetic field direction was once again on the edge of the FIPS FOV. Analogous to the previous orbit, the proton distribution appears to have peaked around the magnetic field direction, which is consistent with a field-aligned flow moving antisunward. Slices through the proton energy distributions during the plasma mantle encounter (Figure 3c) indicate a peak at 0.27 keV, corresponding to a plasma speed of ~230 km s^{-1}.

The proton flux lessened substantially to ~10^6 s^{-1} cm^{-2} as MESSENGER reached the tail lobe proper at 14:47:39 UTC. B remained constant near ~60 nT in the lobe, where the field was mainly in the antisunward direction ($-B_X$) with minimal field fluctuations, since the level of activity considerably decreased without the presence of FTEs or plasma.

4. Cross-Magnetosphere Electric Potential

The plasma's bulk motion from high latitudes toward the central plasma sheet can be used to quantify the cross-magnetosphere electric potential (Φ_{Tail}), which is a measurement of solar wind energy transferred to the magnetosphere. To accomplish this task, we use FIPS measurements, along with the frozen-in flux

condition, $\mathbf{E} = -\mathbf{V}_{E\times B} \times \mathbf{B}$, to calculate E. It is then possible to solve for the electric potential from the equation $\Phi_{Tail} = Ed_{Tail}$, where d_{Tail} is the magnetotail width in the Y_{MSM}-Z_{MSM} plane.

By assuming that the plasma mantle originates at the terminator ($X_{MSM} = 0$), we can calculate L, the length of the mantle in the X_{MSM} direction from the terminator to the downtail location where MESSENGER crossed the magnetopause. Because MESSENGER's orbit was nearly polar, we assume that the spacecraft was moving orthogonal to the magnetopause, in the Z_{MSM} direction, as it traversed through Mercury's southern lobe. From this assumption, we can determine δ, the thickness of the plasma mantle defined as the distance from the magnetopause crossing to MESSENGER's location. Using L and δ (Figure 1a), we may implement a spatial analysis to determine the dispersion wedge angle, θ. Next, we calculate $V_{E\times B}$ from $V_{E\times B} \sim V\theta$ using the small-angle approximation, where V is the plasma mantle velocity calculated from the FIPS proton energy distributions. We solve for E using $V_{E\times B}$ along with B measured in the plasma mantle and then apply d_{Tail} to determine Φ_{Tail}. These calculations were performed over 1 min increments as the spacecraft progressed from the magnetopause to the termination of the plasma mantle. We report the average values for both encounters here.

During the 07:45 UTC orbit, L and δ were calculated to be 2.40 R_M and 0.34 R_M, respectively. The average velocity measured by FIPS was 254 km s^{-1}, from which the average $\mathbf{E}\times\mathbf{B}$ drift velocity is calculated to be $V_{E\times B} \sim 35$ km s^{-1}. This value is multiplied by the average field strength, 52.8 nT, to determine the average cross-tail electric field, $E = 1.91$ mV/m. By taking the tail width to be 5 R_M, consistent with values determined by *Winslow et al.* [2013], we calculate a mean cross-magnetospheric electric potential Φ_{Tail} of ~23 kV.

Applying the same methodology for the 15:45 UTC orbit, we calculate L and δ to be 2.38 R_M and 0.43 R_M, respectively, and find that $V = 269$ km s^{-1} and $V_{E\times B} \sim 47$ km s^{-1}. Using the average field magnitude of 46.4 nT, we determine $E = 2.36$ mV/m in the plasma mantle region. For a tail width of 5 R_M, we calculate a cross-magnetospheric potential Φ_{Tail} of ~29 kV.

There are several uncertainties associated with this methodology: (1) The precise solar wind entry location is unknown. Magnetosheath ions travel along reconnected field lines to enter the magnetosphere through the magnetic cusp [*Raines et al.*, 2014], which is typically upstream of the terminator. Therefore, our estimation of L is likely a lower limit and may increase by ~0.5 R_M, depending on cusp dynamics. (2) Because of single-point measurement constraints, it is impossible to determine the actual width of Mercury's magnetotail during a given orbit. For this reason, we have assumed an average tail width, although this value can increase or decrease by ~2 R_M as Mercury's magnetosphere responds to changing upstream solar wind conditions [*Winslow et al.*, 2013]. (3) There is no way of determining the magnetopause reconnection rate at the time of the plasma mantle encounter. If reconnection were occurring at a high rate for these particular orbits, a condition suggested by the increased FTE activity level, then magnetospheric convection may have been enhanced. (4) Because of FOV constraints, FIPS measures only a fraction of the plasma distribution. Therefore, in a supersonic plasma, the actual flow speed will be higher than the one estimated from the peak in the velocity distribution function [*Gershman et al.*, 2012].

5. Discussion and Conclusions

We have presented the first observations of Mercury's plasma mantle using MESSENGER measurements during two magnetotail traversals on 10 November 2012. FIPS measurements revealed a quasi-continuous transfer of solar wind plasma from the magnetosheath into the high-latitude magnetotail. The plasma mantle was observed for 16 and 21 min intervals during the 07:45 and 15:45 UTC orbits, respectively. A distinct dispersion in the proton energy distribution was observed with increasing distance from the magnetopause due to the $\mathbf{E}\times\mathbf{B}$ drift of low-energy particles toward the central plasma sheet while the higher-energy protons reached the plasma sheet much farther downtail. As particle flux in the plasma mantle decreased, we observed a steady increase in B to maintain pressure balance.

Because of its reconnection dependence, Earth's plasma mantle is correlated with IMF orientation. At Mercury, dayside magnetopause reconnection occurs independent of IMF orientation [*DiBraccio et al.*, 2013], implying that the plasma mantle may be a quasi-persistent feature. Because of single-point measurement constraints we are unable to determine upstream IMF parameters for these two examples. However, the large numbers of FTEs identified during both plasma mantle traversals provide evidence that magnetopause reconnection

was occurring. These intervals are analogous to the "FTE shower" at the magnetopause-magnetosheath interface reported by *Slavin et al*. [2012]. The contribution of FTEs to plasma mantle formation has been only briefly explored at Earth. The model presented by *Sibeck and Siscoe* [1984] implies that FTEs may have a greater effect on magnetospheric dynamics than earlier thought. In any given magnetosphere, this influence is determined by the amount of flux transported by FTEs. At Earth, FTEs contribute only ~2% of the total magnetic flux transport [e.g., *Huang et al*., 2009]. However, in Mercury's magnetosphere, these flux ropes are responsible for at least 30% of the total flux circulated through a single Dungey cycle [*Imber et al*., 2014].

During the two orbits analyzed here, MESSENGER traversed the magnetotail at distances of (2–3) R_M, which is also the expected location of the near-Mercury neutral line [*Slavin et al*., 2009; *DiBraccio et al*., 2015]. The plasma mantle terminated before MESSENGER reached the plasma sheet, which suggests that the solar wind plasma may join the plasma sheet at distances beyond the neutral line. If this were the case, the plasma would be transported tailward and removed by tail reconnection rather than populating the plasma sheet.

Estimates of the electric potential across Mercury's magnetosphere have been performed with several techniques in the past. Following MESSENGER's second Mercury flyby, *Slavin et al*. [2009] determined a potential of ~30 kV using the magnetic field component normal to the magnetopause, B_N, generated by reconnection. *DiBraccio et al*. [2013] performed an extensive survey of dayside magnetopause B_N measurements and found an average potential of 29 kV. After determining the flux content of FTEs at Mercury, *Imber et al*. [2014] applied their short transit times to calculate a cross-polar-cap potential of ~25 kV. In this study, we implemented a new method for calculating Mercury's magnetospheric potential based on measured proton distributions during the two plasma mantle passages examined here. The resulting Φ_{Tail} values are 23 kV and 29 kV, respectively. These results are in good agreement with the previously reported values for Mercury's convection electric field of ~2.0 mV/m by *Slavin et al*. [2009, 2010] derived from the reconnection rate measured at the dayside magnetopause and the short, ~2 min Dungey cycle determined from the brief timescales of tail loading and unloading cycles.

MESSENGER magnetic field and plasma measurements of Mercury's plasma mantle further augment our understanding of this small, but highly active, magnetosphere. The presence of frequent FTEs throughout these encounters supports high reconnection rates and confirms that FTEs are responsible for delivering solar wind into the magnetotail. Statistical studies of larger data sets are needed to determine the sources and sinks for Mercury's plasma sheet as well as its dependence on FTE activity. Nonetheless, these observations of Mercury's plasma mantle reported here provide further evidence that this small magnetosphere is subjected to intense solar wind forcing by the inner heliosphere.

Acknowledgments
The MESSENGER project is supported by the NASA Discovery Program under contracts NASW-00002 to the Carnegie Institution of Washington and NAS5-97271 to The Johns Hopkins University Applied Physics Laboratory. MESSENGER data are publicly available through the Planetary Data System. We thank the two reviewers for providing helpful comments.

The Editor thanks Tomas Karlsson and an anonymous reviewer for their assistance in evaluating this paper.

References

Anderson, B. J., M. H. Acuña, D. A. Lohr, J. Scheifele, A. Raval, H. Korth, and J. A. Slavin (2007), The Magnetometer instrument on MESSENGER, *Space Sci. Rev.*, *131*, 417–450, doi:10.1007/s11214-007-9246-7.

Andrews, G. B., et al. (2007), The Energetic Particle and Plasma Spectrometer instrument on the MESSENGER spacecraft, *Space Sci. Rev.*, *131*, 523–556, doi:10.1007/s11214-007-9272-5.

Daly, P. W., D. J. Williams, C. T. Russell, and E. Keppler (1981), Particle signature of magnetic flux transfer events at the magnetopause, *J. Geophys. Res.*, *86*, 1628–1632, doi:10.1029/JA086ia03p01628.

DiBraccio, G. A., J. A. Slavin, S. A. Boardsen, B. J. Anderson, H. Korth, T. H. Zurbuchen, J. M. Raines, D. N. Baker, R. L. McNutt Jr., and S. C. Solomon (2013), MESSENGER observations of magnetopause structure and dynamics at Mercury, *J. Geophys. Res. Space Physics*, *118*, 997–1008, doi:10.1002/jgra.50123.

DiBraccio, G. A., et al. (2015), MESSENGER observations of flux ropes in Mercury's magnetotail, *Planet. Space Sci.*, *115*, 77–89, doi:10.1016/j.pss.2014.12.016.

Gershman, D. J., T. H. Zurbuchen, L. A. Fisk, J. A. Gilbert, J. M. Raines, B. J. Anderson, C. W. Smith, H. Korth, and S. C. Solomon (2012), Solar wind alpha particles and heavy ions in the inner heliosphere observed with MESSENGER, *J. Geophys. Res.*, *117*, A00M02, doi:10.1029/2012JA017829.

Gershman, D. J., J. A. Slavin, J. M. Raines, T. H. Zurbuchen, B. J. Anderson, H. Korth, D. N. Baker, and S. C. Solomon (2013), Magnetic flux pileup and plasma depletion in Mercury's subsolar magnetosheath, *J. Geophys. Res. Space Physics*, *118*, 7181–7199, doi:10.1002/2013JA019244.

Gershman, D. J., J. A. Slavin, J. M. Raines, T. H. Zurbuchen, B. J. Anderson, H. Korth, D. N. Baker, and S. C. Solomon (2014), Ion kinetic properties in Mercury's pre-midnight plasma sheet, *Geophys. Res. Lett.*, *41*, 5740–5747, doi:10.1002/2014GL060468.

Hill, T. W., A. J. Dessler, and R. A. Wolf (1976), Mercury and Mars: The role of ionospheric conductivity in the acceleration of magnetospheric particles, *Geophys. Res. Lett.*, *3*, 429–432, doi:10.1029/GL003i008p00429.

Huang, C.-S., A. D. DeJong, and X. Cai (2009), Magnetic flux in the magnetotail and polar cap during sawteeth, isolated substorms, and steady magnetospheric convection events, *J. Geophys. Res.*, *114*, A07202, doi:10.1029/2009JA014232.

Imber, S. M., J. A. Slavin, S. A. Boardsen, B. J. Anderson, H. Korth, R. L. McNutt Jr., and S. C. Solomon (2014), MESSENGER observations of large dayside flux transfer events: Do they drive Mercury's substorm cycle?, *J. Geophys. Res. Space Physics*, *119*, 5613–5623, doi:10.1002/2014JA019884.

Le, G., et al. (2008), Flux transfer events simultaneously observed by Polar and Cluster: Flux rope in the subsolar region and flux tube addition to the polar cusp, *J. Geophys. Res.*, *113*, A01205, doi:10.1029/2007JA012377.

Ness, N. F., K. W. Behannon, R. P. Lepping, Y. C. Whang, and K. H. Schatten (1974), Magnetic field observations near Mercury: Preliminary results from Mariner 10, *Science*, *185*, 151–160, doi:10.1126/Science.185.4146.151.

Ness, N. F., K. W. Behannon, R. P. Lepping, and Y. C. Whang (1975), Magnetic field of Mercury confirmed, *Nature*, *255*, 204–205, doi:10.1038/255204a0.

Ogilvie, K. W., J. D. Scudder, R. E. Hartle, G. L. Siscoe, H. S. Bridge, A. J. Lazarus, J. R. Asbridge, S. J. Bame, and C. M. Yeates (1974), Observations at Mercury encounter by the Plasma Science Experiment on Mariner 10, *Science*, *185*, 145–151, doi:10.1126/science.185.4146.145.

Ogilvie, K. W., J. D. Scudder, V. M. Vasyliunas, R. E. Hartle, and G. L. Siscoe (1977), Observations at the planet Mercury by the Plasma Electron Experiment: Mariner 10, *J. Geophys. Res.*, *82*, 1807–1824, doi:10.1029/JA082i013p01807.

Paschmann, G., G. Haerendel, I. Papamastorakis, N. Sckopke, S. J. Bame, J. T. Gosling, and C. T. Russell (1982), Plasma and magnetic field characteristics of magnetic flux transfer events, *J. Geophys. Res.*, *87*, 2159–2168, doi:10.1029/JA087ia04p02159.

Pilipp, W. G., and G. Morfill (1978), The formation of the plasma sheet resulting from plasma mantle dynamics, *J. Geophys. Res.*, *83*, 5670–5678, doi:10.1029/JA083ia12p05670.

Potter, A., and T. Morgan (1985), Discovery of sodium in the atmosphere of Mercury, *Science*, *229*, 651–653.

Potter, A., and T. Morgan (1986), Potassium in the atmosphere of Mercury, *Icarus*, *67*, 336–340.

Raines, J. M., J. A. Slavin, T. H. Zurbuchen, G. Gloeckler, B. J. Anderson, D. N. Baker, H. Korth, S. M. Krimigis, and R. L. McNutt Jr. (2011), MESSENGER observations of the plasma environment near Mercury, *Planet. Space Sci.*, *59*, 2004–2015, doi:10.1016/j.pss.2011.02.004.

Raines, J. M., et al. (2013), Distribution and compositional variations of plasma ions in Mercury's space environment: The first three Mercury years of MESSENGER observations, *J. Geophys. Res. Space Physics*, *118*, 1604–1619, doi:10.1029/2012JA018073.

Raines, J. M., D. J. Gershman, J. A. Slavin, T. H. Zurbuchen, H. Korth, B. J. Anderson, and S. C. Solomon (2014), Structure and dynamics of Mercury's magnetospheric cusp: MESSENGER measurements of protons and planetary ions, *J. Geophys. Res. Space Physics*, *119*, 6587–6602, doi:10.1002/2014JA020120.

Rosenbauer, H., H. Grunwaldt, M. D. Montgomery, G. Paschmann, and N. Sckopke (1975), Heos-2 plasma observations in distant polar magnetosphere—Plasma mantle, *J. Geophys. Res.*, *80*, 2723–2737, doi:10.1029/JA080i019p02723.

Russell, C. T., and R. C. Elphic (1978), Initial ISEE Magnetometer results: Magnetopause observations, *Space Sci. Rev.*, *22*, 681–715.

Russell, C. T., and R. C. Elphic (1979), ISEE observations of flux transfer events at the dayside magnetopause, *Geophys. Res. Lett.*, *6*, 33–36, doi:10.1029/GL006i001p00033.

Sckopke, N., and G. Paschmann (1978), The plasma mantle. A survey of magnetotail boundary layer observations, *J. Atmos. Terr. Phys.*, *40*, 261–278, doi:10.1016/0021-9169(78)90044-2.

Sckopke, N., G. Paschmann, H. Rosenbauer, and D. H. Fairfield (1976), Influence of the interplanetary magnetic field on occurrence and thickness of plasma mantle, *J. Geophys. Res.*, *81*, 2687–2691, doi:10.1029/JA081i016p02687.

Sibeck, D. G., and G. L. Siscoe (1984), Downstream properties of magnetic flux transfer events, *J. Geophys. Res.*, *89*, 709–715, doi:10.1029/JA089ia12p10709.

Simpson, J. A., J. H. Eraker, J. E. Lamport, and P. H. Walpole (1974), Electrons and protons accelerated in Mercury's magnetic field, *Science*, *185*, 160–166, doi:10.1126/Science.185.4146.160.

Siscoe, G. L., and E. Sanchez (1987), An MHD model for the complete open magnetotail boundary, *J. Geophys. Res.*, *92*, 7405–7412, doi:10.1029/JA092ia07p07405.

Siscoe, G. L., N. F. Ness, and C. M. Yeates (1975), Substorms on Mercury?, *J. Geophys. Res.*, *80*, 4359–4363, doi:10.1029/JA080i031p04359.

Slavin, J. A., E. J. Smith, D. G. Sibeck, D. N. Baker, R. D. Zwickl, and S. I. Akasofu (1985), An ISEE-3 study of average and substorm conditions in the distant magnetotail, *J. Geophys. Res.*, *90*, 875–895, doi:10.1029/JA090ia11p10875.

Slavin, J. A., et al. (2008), Mercury's magnetosphere after MESSENGER's first flyby, *Science*, *321*, 85–89, doi:10.1126/Science.1159040.

Slavin, J. A., et al. (2009), MESSENGER observations of magnetic reconnection in Mercury's magnetosphere, *Science*, *324*, 606–610, doi:10.1126/Science.1172011.

Slavin, J. A., et al. (2010), MESSENGER observations of extreme loading and unloading of Mercury's magnetic tail, *Science*, *329*, 665–668, doi:10.1126/Science.1188067.

Slavin, J. A., et al. (2012), MESSENGER observations of a flux-transfer-event shower at Mercury, *J. Geophys. Res.*, *117*, A00M06, doi:10.1029/JA017926.

Winslow, R. M., B. J. Anderson, C. L. Johnson, J. A. Slavin, H. Korth, M. E. Purucker, D. N. Baker, and S. C. Solomon (2013), Mercury's magnetopause and bow shock from MESSENGER Magnetometer observations, *J. Geophys. Res. Space Physics*, *118*, 2213–2227, doi:10.1002/jgra.50237.